

Ab initio study of reflectance anisotropy spectra of a sub-monolayer oxidized Si(100) surface

André Incze

*Istituto Nazionale per la Fisica della Materia,
Dipartimento di Fisica dell'Università di Milano, via Celoria 16,
I-20133 Milano, Italy and Istituto Nazionale per la Fisica
della Materia e Dipartimento di Fisica dell'Università
di Roma "Tor Vergata", Via della Ricerca Scientifica, I-00133 Roma, Italy*

Rodolfo Del Sole

*Istituto Nazionale per la Fisica della Materia e Dipartimento di Fisica dell'Università
di Roma "Tor Vergata", Via della Ricerca Scientifica, I-00133 Roma, Italy*

Giovanni Onida

*Istituto Nazionale per la Fisica della Materia,
Dipartimento di Fisica dell'Università di Milano,
via Celoria 16, I-20133 Milano, Italy*

(Dated: May 23, 2019)

Abstract

The effects of oxygen adsorption on the reflectance anisotropy spectrum (RAS) of reconstructed Si(100):O surfaces at sub-monolayer coverage (first stages of oxidation) have been studied by an *ab initio* DFT-LDA scheme within a plane-wave, norm-conserving pseudopotential approach. Dangling bonds and the main features of the characteristic RAS of the clean Si(100) surface are mostly preserved after oxidation of 50% of the surface dimers, with some visible changes: a small red shift of the first peak, and the appearance of a distinct spectral structure at about 1.5 eV. The electronic transitions involved in these changes have been analyzed through state-by-state and layer-by-layer decompositions of the RAS. We suggest that new interplay between present theoretical results and reflectance anisotropy spectroscopy experiments could lead to further clarification of structural and kinetic details of the Si(100) oxidation process in the sub-monolayer range.

PACS numbers: 78.68.+m, 71.15.Qe, 73.20.-r, 78.40.-q

The developments in the capability to monitor and to control oxidation of the silicon (100) surface at an atomic-scale resolution are a very important issue in semiconductor device technology. In fact, high quality gate insulators thinner than 2nm are today required, due to the continuous downscaling of the metal-oxide-semiconductor (MOS) devices (see, e.g., Ref. [1]).

In the last two decades the adsorption of oxygen on silicon surfaces has been extensively studied, from both experimental and theoretical points of view. In particular, the effects induced by oxidation on the optical properties of the silicon surfaces are being thoroughly studied since the mid eighties [2, 3]. It has been known since then that O_2 adsorption is dissociative, and that preferred final adsorption sites for O atoms are Si-Si bond-bridge positions. More recently, it has been shown that in the case of Si(100) the most favorable adsorption sites for O are the dimer-bridge, and the backbond site of the down atom of the surface dimer [4, 5]. The latter site is slightly favored over the former when insertion of an isolated O atom is considered, but with two oxygen atoms the most favorable configuration is that with one oxygen inserted into the down atom backbond, and the other inserted into the dimer bond [6, 7]. It is also known that, during the first stages of oxidation, O_2 adsorption and O migration to the backbonds proceed as barrierless (or almost barrierless) reactions, as demonstrated by both experimental [8] and theoretical [9, 10] works. Moreover, experiments show evidence that further Si(100) oxidation proceeds in a layer-by-layer process, giving rise to an oscillatory effect in the surface anisotropy, which has been detected by "in situ" reflectance anisotropy spectroscopy measurements [11, 12]. The phenomenon of the growth of a SiO_2 layer over the Si(100) surface, and the related problem of the properties of the Si- SiO_2 interface, have received most of the attention, and several calculations of structural and electronic properties of the interface are available [13, 14]. However, what happens in the very first stages of oxidation (below 1 ML coverage) is still poorly known: oxidation of the second layer starts soon [15], and recent experimental works [12, 16] do not focus on the formation of the first layer, which is completed in a very short time (less than 1 second) at the experimentally used O_2 partial pressures [39]. Since reflectance anisotropy spectroscopy is a very sensitive technique, which in the case of the clean Si(100) surface is able to detect small structural details [17, 18], and –in contrast with other characterization techniques based on electrons– can be used "in situ" to monitor the process under manufacturing conditions (where the O_2 pressure is typically in the range from 10^2 to 10^5 Pa), we suggest, with the

present work, a possible application of reflectance anisotropy spectroscopy to shed light on the structural and kinetic details of the Si(100) oxidation process in the sub-monolayer range.

Our aim is to study in a detailed and quantitative way the changes on the RAS features induced by very low concentrations of chemisorbed oxygen on the Si(100) surface. To this scope, a layer-resolved analysis of the most relevant low-energy spectral features will be presented.

I. THEORY

The RAS is defined as the difference between the normalized reflectivities measured at normal incidence, for two orthogonal polarizations of light. Throughout this paper, the surface is perpendicular to the x axis, and the z direction is perpendicular to the Si-Si dimers of the reconstructed Si(100) surface. RAS is hence measured, as a function of the photon energy, as $(\Delta R_y/R) - (\Delta R_z/R)$, where R is the (isotropic) Fresnel reflectivity. Describing the surface within a repeated slab geometry, one can express $\Delta R_i/R$, ($i = y, z$) for normally incident light as [19]:

$$\frac{\Delta R_i}{R} = \frac{4\omega}{c} \text{Im} \frac{4\pi\alpha_{ii}^{hs}(\omega)}{\epsilon_b(\omega) - 1}, \quad (1)$$

where i is the polarization direction, $\alpha_{ii}^{hs}(\omega)$ are the diagonal terms of the half-slab polarizability tensor, and $\epsilon_b(\omega)$ is the complex bulk dielectric function.

If the slab has a center of inversion or a mirror plane parallel to the surface ($x \rightarrow -x$ symmetry, in our case), the imaginary part of $\alpha_{ii}^{hs}(\omega)$ can be written, in the single-quasiparticle approximation, as:

$$\text{Im}[4\pi\alpha_{ii}^{hs}(\omega)] = \frac{4\pi^2 e^2}{\omega^2 A} \sum_{\vec{k}} \sum_{v,c} |V_{v\vec{k},c\vec{k}}^i|^2 \delta(E_{c\vec{k}} - E_{v\vec{k}} - \hbar\omega), \quad (2)$$

where $V_{v\vec{k},c\vec{k}}^i$ are the matrix element of the velocity operator between occupied (v) and empty (c) slab eigenstates at the point \vec{k} in the surface Brillouin zone [20]. "A" is the slab surface area, while $E_{c\vec{k}}$ and $E_{v\vec{k}}$ are conduction and valence energy eigenvalues, taken as representative of quasiparticle energies. Neglecting the pseudopotential nonlocality [21], the velocity operator can be replaced by the momentum operator divided by the electronic mass,

whose matrix elements $P_{v\vec{k},c\vec{k}}^i$ are easy to evaluate in the plane-wave basis. If the slab has two identical surfaces, α_{ii}^{hs} is simply obtained by dividing by two the polarizability of the full slab. There are many cases, however, where one needs to single out the contributions coming from an individual half of the slab, or from regions situated at different depths below the surface. This problem has been recently discussed by some of us [22] and by others [23, 24], and can be solved by introducing a real-space cutoff in the definition of the matrix elements.

This method proved itself very useful for separating surface contributions from bulk and subsurface ones in optical spectra, and has already been applied to the case of the clean Si(100) reconstructed surface [22]. In the real-space cutoff scheme, modified matrix elements $\tilde{P}_{v\vec{k},c\vec{k}}^i$ are needed, which incorporate a function $\theta(x)$ switching from 1 inside the selected region to zero outside the selected region. $\tilde{P}_{v\vec{k},c\vec{k}}^i$ are defined as:

$$\tilde{P}_{v\vec{k},c\vec{k}}^i = -i\hbar \int d^3\vec{r} \Psi_{v\vec{k}}^*(\vec{r}) \theta(x) \frac{\partial}{\partial r_i} \Psi_{c\vec{k}}(\vec{r}). \quad (3)$$

The imaginary part of the polarizability is hence given by [22]:

$$Im[\alpha_{ii}^{cut}] = \frac{2\pi e^2}{m^2 \omega^2 A} \sum_{\vec{k}} \sum_{v,c} [P_{v\vec{k},c\vec{k}}^i]^* \tilde{P}_{v\vec{k},c\vec{k}}^i \delta(E_{c\vec{k}} - E_{v\vec{k}} - \hbar\omega), \quad (4)$$

where both $\tilde{P}_{v\vec{k},c\vec{k}}^i$ and $P_{v\vec{k},c\vec{k}}^i$ (the standard momentum matrix element, calculated without the cut-off function) appear. Working in the reciprocal space, the evaluation of $\tilde{P}_{v\vec{k},c\vec{k}}^i$ requires a double sum over the reciprocal lattice vectors $\{\vec{G}\}$ ([22], [40]), in contrast to the single sum which yields $P_{v\vec{k},c\vec{k}}^i$.

II. COMPUTATIONAL DETAILS

Electronic wavefunctions and eigenvalues are obtained within the local density approximation (LDA) to density-functional theory [25, 26] using a plane-waves basis set. The exchange-correlation energy is evaluated according to the Ceperley and Alder results [27] as parametrized by Perdew and Zunger [28]. The ion-electron interaction is represented by norm-conserving pseudopotentials. Special attention was devoted to the generation of a good norm-conserving pseudopotential for oxygen, in order to achieve an high transferability without requiring too many plane waves for convergence. To this aim, we adopted the Hamann scheme [29], and optimized the core radii in order to find the best compromise between the basis set convergence and transferability. The latter was checked not only against

logarithmic derivatives, but also performing explicit atomic calculations in several excited configurations. More extensive pseudopotential tests have been performed on three small molecules (SiO , H_2SiO , Si_2O) and on the α -quartz crystalline phase of silica, in order to check the convergence of their structural and electronic properties with respect to the basis set (number of plane waves). As a result, the theoretical length of the Si-O bond is found to converge (within 1%) already at a 30 Ry cutoff for all three molecules. The theoretical values of 1.51 Å (SiO) and 1.52 Å (H_2SiO) compare well with the experimental ones (1.51 Å [30] and 1.515 Å [31] respectively). Concerning α -quartz, the calculated lattice constant at 30 Ry is 4.87 Å, to be compared with the experimental value of 4.916 Å [32].

The $\text{Si}(100)\text{-p}(2\times 2)$ reconstructed surface was simulated by a repeated slab of twelve silicon layers and four layers of vacuum. First, the clean surface structure has been determined by a full structural optimization (keeping only the central four Si layers as fixed), using the Broyden-Fletcher-Goldfarb-Shanno minimization algorithm as implemented in the Abinit code [33] until the residual forces acting on each atom are less than 0.01 eV/Å. The resulting structure was in agreement with previous results [34], with a dimer buckling of 0.79 Å. Two O atoms were then adsorbed on each of the two slab surfaces (in order to preserve the inversion symmetry), which corresponds to a 0.5 ML oxidation. Based on previous *ab initio* calculations of oxygen adsorption on the $\text{Si}(100)$ surface [6, 7], we have chosen the most stable configuration after barrierless dissociation of the molecule: one O atom is in bridge position on the dimer, and the other is in a bridge bonded position on the backbond site of the lower atom of the dimer.

III. RESULTS

After oxygen adsorption on the dimer and backbond bridge sites (Fig. 1), and a new full structural relaxation, one of the surface Si-Si dimers is broken (see Tab. I: the dimer length after oxidation becomes 3.06 Å). Concerning the length of the oxidized Si backbond, we obtain 2.53 Å after O adsorption, to be compared with the 2.60 Å reported in Ref. [4]. The structural relaxation remains limited to the immediate neighbouring of the O atom, since subsurface layers (2nd and 3rd silicon layer) are not affected appreciably. The buckling of the non-oxidized dimer, which is expected to be stabilized by O adsorption [5], increases only very slightly, passing from 0.79 to 0.81 Å.

To compute optical spectra, the ground state calculation must be followed by a calculation of bandstructure energies and wavefunctions over a dense mesh in the irreducible wedge of the Brillouin zone, for both occupied and empty states. To this aim, we calculated Kohn–Sham eigenvectors and eigenvalues using the Arnoldi algorithm [35], for all states up to 12 eV above the highest occupied state (i.e., about 250 empty states above the 108 filled ones) in each \vec{k} -point.

Fig. 2 shows the computed bandstructure, near the Fermi level, for both the clean and the oxidized surfaces, along the Γ KJ Γ path in the irreducible wedge of the surface Brillouin zone. For the clean surface, results are in excellent agreement with previous *ab initio* DFT-LDA calculations [34] on the Si(100)–p(2x2) surface. We note the strong dispersion along Γ K and KJ for the surface bands arising from the dangling bonds which form π (bonding) and π^* (antibonding) states. This large dispersion is associated with a non-negligible interaction between adjacent silicon dimers in the direction perpendicular to the dimer axis [36, 37].

After oxidation, the direct gap at Γ increases from 0.2 to 0.4 eV. However, surface states are still localized on DBs, as can be seen from a plot (not shown) of their charge densities. Even the oxidized dimers show distinct filled and empty DB-like surface states. The band dispersion in the direction perpendicular to dimers becomes smaller, which can be explained by a weakening of the interaction between adjacent dimers (in our case, an oxidized and a non oxidized one), as a consequence of oxidation. Oxidation also lifts the initial degeneracy of surface bands at the K corner of the surface Brillouin zone.

Optical spectra have been computed according to Eq. (4), using increasingly large sets of \vec{k} -points (up to 162). The following Monkhorst–Pack [38], \vec{k} -point meshes were considered in the upper half of the (2x2) Surface Brillouin Zone: 5x5, 7x7, 9x9, 11x11 and 18x9. In the energy window 0–3.5 eV, the 9x9 mesh is sufficient to achieve convergence, superimposing a small Gaussian broadening (75 meV) to the calculated spectrum. Similarly, in the range between 6 and 12 eV, the 11x11 mesh is sufficient, with the same small broadening. The intermediate energy window, between 3.5 and 6 eV, is the most slowly convergent one. Indeed, a fully converged RAS in this region can only be obtained by increasing the broadening up to 250 meV, with the largest \vec{k} -point sets used (11x11 and 18x9). These results are summarized in Fig. 3.

Comparing the RAS of the oxidized and clean surfaces up to 1.8 eV two differences come into evidence: i) after oxygen adsorption, there is a redshift by 0.2 eV of the main transition

peak of the clean surface, and ii) a new structure appears between 1.4 and 1.75 eV (see Fig. 4). However, the overall RAS lineshape does not undergo qualitative changes.

In order to clarify the origin and nature of these modifications, we have performed a layer-by-layer analysis of the RAS according to Eq. (3) and Eq. (4), applying the real-space cutoff method described in Ref. [22]. This allows one to quantify the contribution to the RAS originated in the different surface and subsurface regions. We divided our slab in five slices: the first four (starting from the middle of the slab) containing only silicon atoms, and the last one including surface dimers, oxygen atoms, and the subsurface Si atoms bonded to the surface dimers, as shown in Fig. 5. For the last slice, the cutoff region extends up to a distance of about 1 Å above the surface. The resulting spectra are displayed in Fig. 6: as expected, the reflectance anisotropy signal coming from slice 1 and slice 2 is almost zero up to 3.0 eV (i.e., in the whole region below the bulk Si direct gap), coherently with the fact that they are bulk representative. The presence of the surface starts to be felt in the 3rd slice, where the two main negative RAS peaks, characteristic of the clean surface, start to appear (at about 1 and 3 eV, respectively). Slice 4 gives a contribution very similar to slice 3, with a larger strength of the 1.0 eV peak. The latter peak is also strongly present in the topmost slice contribution, together with the 3 eV one. An analysis of the localization of electronic states involved in strongest dipole allowed transitions for the 1.0 eV peak show almost no contributions from electronic states involving O atoms. Indeed, the states which originate this peak are valence states corresponding mainly to dangling bonds localized on the upper Si atom of the oxidized dimer, and conduction states corresponding mainly to p_x -like orbitals of the lower silicon atom of the non-oxidized dimer. However, besides the two main peaks at 1 and 3 eV, the topmost slice also contributes with a new structure, located at about 1.5 eV, which does not appear in slice 3 and slice 4 contributions. Empty states involved in the transitions responsible for this feature are in fact found to be strongly localized on the lower Si atom of the Si-O-Si bridge (broken dimer), and on the O atoms themselves (p -like orbitals), so this feature represents a sort of oxygen signature.

In order to obtain deeper insight on the electronic states involved in the main spectral structures, we have singled out, from the whole summation appearing in Eq. (4), the contributions which give the largest oscillator strength and the larger anisotropy, restricted to well-defined energy windows centered on the main low-energy peaks of the imaginary part of the slab polarizability tensor. To this aim, we have selected three energy windows,

labeled with A, B and C (Fig. 7). based on the plot of the imaginary part of the half-slab polarizability for light polarization perpendicular (z) and parallel (y) to the silicon dimers. In each region, the contribution coming from each \vec{k} -point and band pairs (vc) have been sorted on the basis of two criteria: the value of the squared modulus $|P_{v\vec{k},c\vec{k}}^z|^2$, and the value of the anisotropy calculated as $(|P_{v\vec{k},c\vec{k}}^z|^2 - |P_{v\vec{k},c\vec{k}}^y|^2)/(|P_{v\vec{k},c\vec{k}}^z|^2 + |P_{v\vec{k},c\vec{k}}^y|^2)$. As a result, only the uppermost 4 valence states (labeled: 105–108) and the lowest 4 conduction states (labeled: 109–112) are found to be the main responsables for the strongest optical transitions, with $107 \rightarrow 109$ and $108 \rightarrow 109$ contributing to peak A ([0.8,0.9] eV), and $107+108 \rightarrow 110+111$ contributing to peak B ([1.0,1.15] eV), while peak C ([1.40,1.75] eV) is due to the transitions $106 \rightarrow 111$ and $105 \rightarrow 112$, as illustrated in Fig. 7.

This result is confirmed by the comparison of the full RAS with a spectrum computed including only this set of 4 valence and 4 conduction states (i.e., based on just 16 out of 27216 v - c transitions): in the energy window between 0 and 1.8 eV all main features of the RAS are reproduced, apart for small difference in intensities (Fig. 8).

IV. CONCLUSIONS

In conclusion, we have studied the very first stage of oxidation of Si(100)-p(2x2), at a coverage of 0.5 ML, showing that oxidation of one of the two Si-Si dimers of the p(2x2) unit cell does not change dramatically the RAS shape, despite the breaking of the dimer and the large flattening of the lowest conduction band, which reflects the weakening of the dimer-dimer interaction along the direction perpendicular to the dimer axis. In particular, the negative peak at 3.7 eV does not disappear (see footnote 39). However, oxidation of one dimer gives rise to distinguishable effects on the RAS in the lowest energy region (0 to 1.8 eV), which can be understood in terms of transitions between the four highest valence bands and the four lowest conduction bands of the slab, localized essentially on dangling bonds of silicon atoms, belonging to both types of dimers (oxidized and non-oxidized). These effects are essentially summarized by a redshift of about 0.2 eV of the first RAS negative peak, disappearance of the small structures below 1.0 eV, typical of the clean surface, and appearance of a new structure at 1.5 eV, which can be seen as an "oxygen signature". The latter can be clearly separated from extra artificial oscillations induced by the discreteness of the Brillouin zone sampling, when a sufficiently large number of \vec{k} -points is used. The

shift of the first negative peak is strongly linked to the structural surface relaxation which follows oxygen adsorption, and becomes larger if the relaxation is not complete. A layer-by-layer analysis of the RAS shows that the 1.5 eV structure is extremely surface-localized (topmost 2.64 Å), while the origin of the two main negative peaks also extends somehow to the subsurface region (topmost 5.42 Å). We predict that the appearance of this feature should be detectable in reflectance anisotropy spectroscopy experiments on Si(100) in the sub-monolayer range (i.e. at quite lower oxygen exposure than in most presently available experimental data).

On the basis of the present results, we speculate that also 1 ML of O, as far as oxygen stays at the bridge sites without saturating the DBs, should not destroy the main RAS features of the clean surface. It is hence an open question which O geometry and coverage will eventually lead to their quenching.

V. ACKNOWLEDGEMENTS

We acknowledge the European Community for financial support under the NANOQUANTA project (contract no. NMP4-CT-2004-500198), and the Italian “Ministero dell’Istruzione, dell’Università e della Ricerca” for financial support within COFIN 2002. A. Incze also acknowledges support through the EEC under contract no. HPRNT-CT-2000-00167 (Univ. Tor Vergata, Roma). We would like to thank C. Hogan, M. Palummo, and M. Gatti for useful discussions, and N. Manini for a careful reading of the manuscript. Computer facilities at CINECA granted by INFN (Project ID n. 239488704824) are gratefully acknowledged.

-
- [1] I. J. R. Baumvol, Surf. Sci. Rep. **36**, 1 (1999).
 - [2] E. G. Keim, L. Wolterbeek, and A. van Silfhout, Surf. Sci. **180**, 565 (1987).
 - [3] A. Selloni, P. Marsella, and R. Del Sole, Phys. Rev. B **33**, 8885 (1986).
 - [4] T. Uchiyama and M. Tsukada, Surf. Sci. **357**, 509 (1996).
 - [5] T. Uchiyama and M. Tsukada, Phys. Rev. B **53**, 7917 (1996).
 - [6] T. Uchiyama, T. Uda, and K. Terakura, Surf. Sci. **433**, 896 (1999).
 - [7] Y. Widjaja and C. B. Musgrave, J. Chem. Phys. **116**, 5774 (2002).

- [8] H. Watanabe, K. Kato, T. Uda, K. Fujita, M. Ichikawa, T. Kawamura, and K. Terakura, Phys. Rev. Lett. **80**, 345 (1998).
- [9] K. Kato, T. Uda, and K. Terakura, Phys. Rev. Lett. **80**, 2000 (1998).
- [10] K. Kato and T. Uda, Phys. Rev. B **62**, 15978 (2000).
- [11] T. Yasuda, S. Yamasaki, M. Nishizawa, N. Miyata, A. Shklyaev, M. Ichikawa, T. Matsudo, and T. Ohta, Phys. Rev. Lett. **87**, 037403 (2001).
- [12] T. Matsudo, T. Ohta, T. Yasuda, M. Nishizawa, N. Miyata, S. Yamasaki, A. A. Shklyaev, and M. Ichikawa, J. of Appl. Phys. **91**, 3637 (2002).
- [13] A. Pasquarello, M. S. Hybertsen, and R. Car, Nature **396**, 58 (1998).
- [14] T. Nakayama and M. Murayama, Appl. Phys. Lett. **77**, 4286 (2000).
- [15] K. Nakajima, Y. Okazaki, and K. Kimura, Phys. Rev. B **63**, 113314 (2001).
- [16] T. Yasuda, N. Kumagai, M. Nishizawa, S. Yamasaki, H. Oheda, and K. Yamabe, Phys. Rev. B **67**, 195338 (2003).
- [17] R. Shioda and J. van der Weide, Phys. Rev. B **57**, R6823 (1998).
- [18] U. Rossow, L. Mantese, and D. E. Aspnes, J. Vac. Sci. Technol. B, **14**, 3070 (1996).
- [19] F. Manghi, R. Del Sole, A. Selloni, and E. Molinari, Phys. Rev. B **41**, 9935 (1990).
- [20] R. Del Sole, *Reflectance Spectroscopy-Theory*, in *Photonic Probes of Surfaces*, edited by P. Halevi, (Elsevier, Amsterdam 1995), p.131.
- [21] see e.g.: A. Marini, G. Onida, and R. Del Sole, Phys. Rev. B **64**, 195125 (2001).
- [22] C. Hogan, R. Del Sole, and G. Onida, Phys. Rev. B **68**, 035405 (2003).
- [23] C. Castillo, B. S. Mendoza, W. G. Schmidt, P. H. Hahn, and F. Bechstedt, Phys. Rev. B **68**, 041310 (2003).
- [24] P. Monachesi, M. Palummo, R. Del Sole, A. Grechnev, and O. Eriksson, Phys. Rev. B **68**, 035426 (2003).
- [25] P. Hohenberg and W. Kohn, Phys. Rev. **136**, B864 (1964).
- [26] W. Kohn and L.J. Sham, Phys. Rev. **140**, A1133 (1965).
- [27] D. M. Ceperley and B. J. Alder, Phys. Rev. Lett. **45**, 566 (1980).
- [28] J. P. Perdew and A. Zunger, Phys. Rev. B **23**, 5048 (1981).
- [29] G. B. Bachelet, D. R. Hamann, and M. Schlüter, Phys. Rev. B **26**, 4199 (1982).
- [30] *Molecular spectra and molecular structure*, by G. Herzberg, 2nd edition, New York, Van Nostrand Reinhold, (1950).

- [31] M. Bogey, B. Delacroix, A. Walters, and J.-C. Guillemin, J. Mol. Spectrosc. **175**, 421 (1996).
- [32] L. Levien, C.T. Prewitt, and D. J. Weidner, Am. Mineral. **65**, 920 (1980).
- [33] X. Gonze, J.-M. Beuken, R. Caracas, F. Detraux, M. Fuchs, G.-M. Rignanese, L. Sindic, M. Verstraete, G. Zerah, F. Jollet, M. Torrent, A. Roy, M. Mikami, Ph. Ghosez, J.-Y. Raty, and D. C. Allan, Comput. Mat. Sci. **25**, 478 (2002).
- [34] A. Ramstad, G. Brocks, and P. J. Kelly, Phys. Rev. B **51**, 14504 (1995).
- [35] *ARPACK Users' Guide: Solution of Large-Scale Eigenvalue Problems with Implicitly Restarted Arnoldi Methods*, by R. B. Lehoucq, D. C. Sorensen, and C. Yang, edited by SIAM, Philadelphia, (1998). *ARPACK-Arnoldi Package*, www.caam.rice.edu/software/ARPACK.
- [36] M. Palummo, G. Onida, R. Del Sole, and B. S. Mendoza, Phys. Rev. B **60**, 2522 (1999).
- [37] C. Kress, A. Shkrebtii, and R. Del Sole, Surf. Sci. **377**, 398 (1997).
- [38] J. D. Pack and H. J. Monkhorst, Phys. Rev. B **16**, 1748 (1977).
- [39] As a consequence, the well-known surface originating negative RAS peak at about 3.7 eV disappears [12].
- [40] Because of the double sum, the computation of the matrix elements using the cutoff technique can become time consuming, especially when a high cutoff energy is required for convergence. We have checked convergence of the matrix elements calculation over the number of \vec{G} -vectors included in the sum. We have obtained that 4000 \vec{G} -vectors are enough for achieving convergence, approximatively 1/5 of the initial basis size.

surface	$\alpha_1(^{\circ})$	$d_1(\text{\AA})$	$\alpha_2(^{\circ})$	$d_2(\text{\AA})$
clean	19.2	2.33	19.2	2.33
oxidized	11	3.06	20.27	2.34
	(-43%)	(+31%)	(+6%)	(0.4%)

TABLE I: Structural changes (Si-Si buckling angle α and dimer length d) at the p(2x2) reconstructed Si(100) surface, subsequent to 0.5 ML oxidation. Subscript 1 corresponds to the dimer which undergoes oxidation, while subscript 2 to the dimer which remains clean. In parenthesis, variations in % with respect to the clean surface. The buckling angles in the case of the clean surface are the averages of two slightly different angles for the two dimers [34].

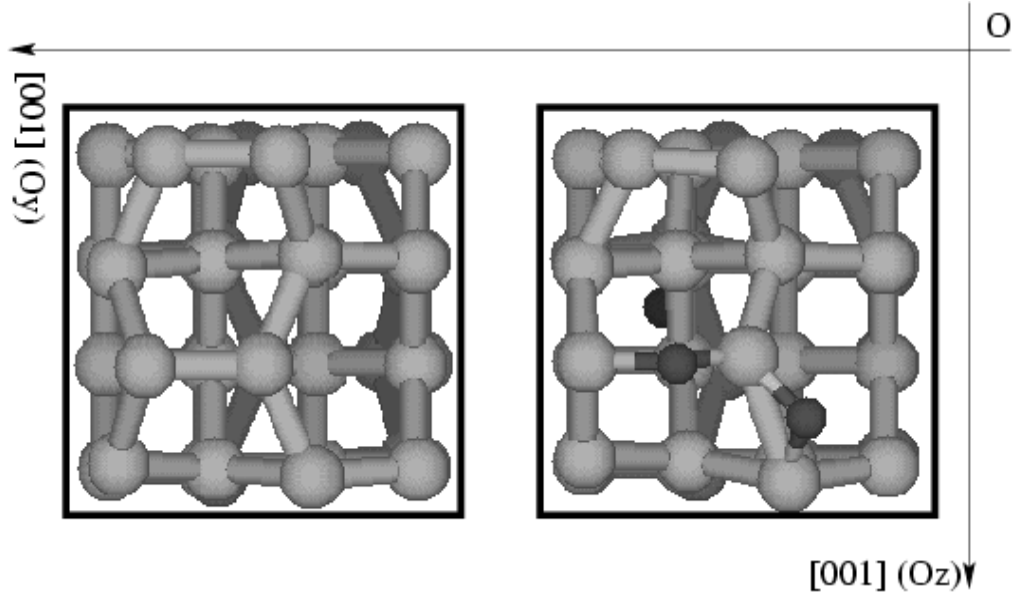


FIG. 1: Top view of the slab after structural optimization, for the clean (left) and oxidized (right) Si(100)-p(2x2) surfaces. The x axis is perpendicular to the surface, and Si-Si surface dimers are oriented along the y axis.

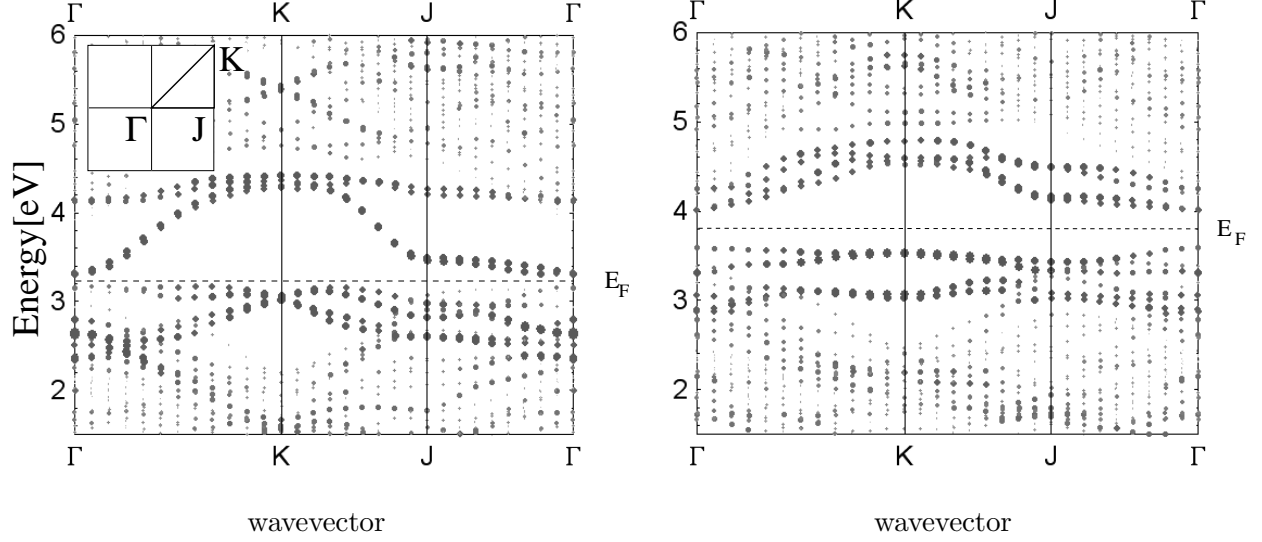


FIG. 2: Surface bandstructure for Si(100)- $p(2 \times 2)$, clean (left) and 0.5 ML oxidized (right). Bold dots are used for states which are spatially localized at the surface (integral of $|\Psi_{n\vec{k}}(\vec{r})|^2$ over the 2 topmost layers larger than 0.5). The Fermi level has been taken in the middle of the surface band gap.

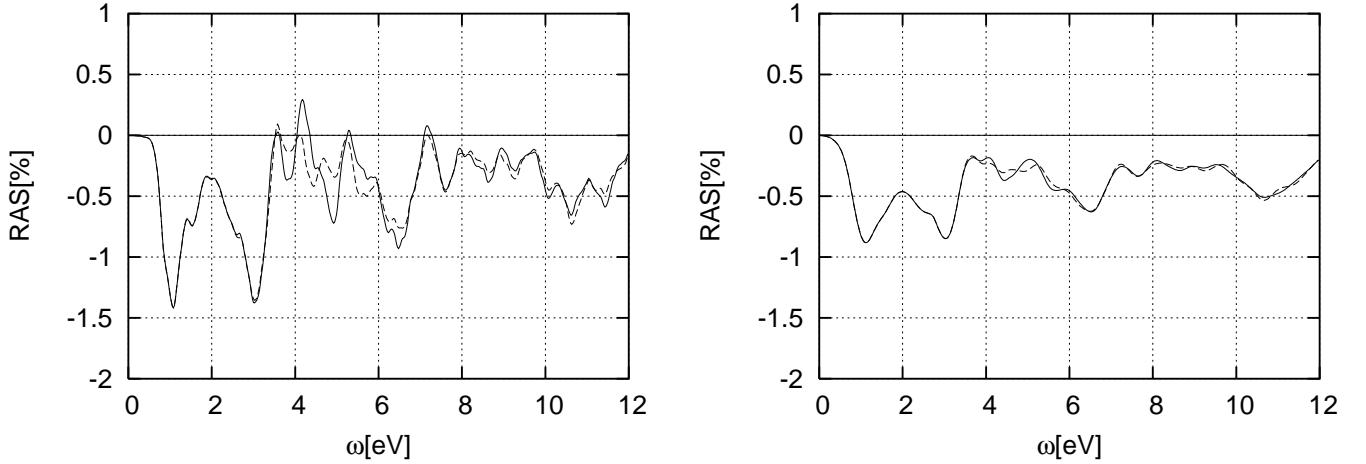


FIG. 3: Convergence of the RAS of the 0.5 ML oxidized Si(100)- $p(2 \times 2)$ surface with respect to the Brillouin zone sampling. Left: spectra calculated with the 9x9 and 18x9 grids (continuous and dashed lines respectively), using a gaussian broadening of 75 meV. Right: spectra calculated with the 11x11 and 18x9 grids (continuous and dashed lines respectively), using a gaussian broadening of 250 meV.

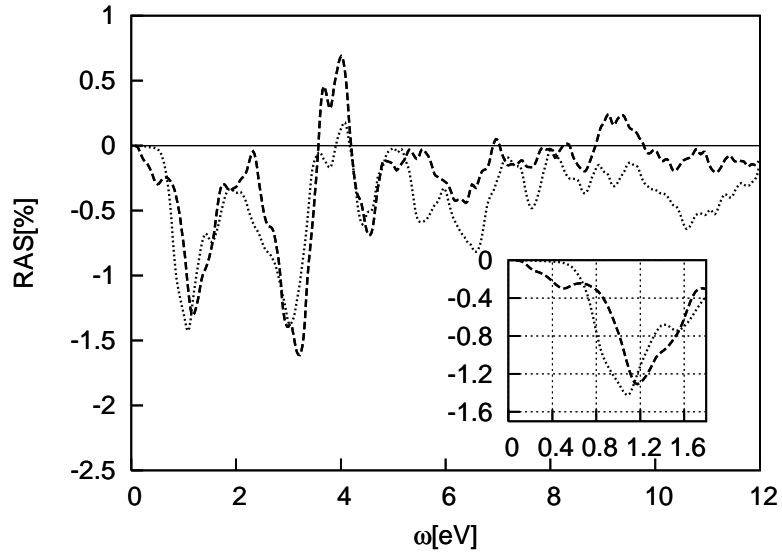


FIG. 4: Effects of the 0.5 ML oxidation on the RAS of Si(100)-p(2x2): clean surface (dashed line) versus oxidized one (dotted line). In the inset, detail of the low-energy region. A gaussian broadening of 75 meV has been used.

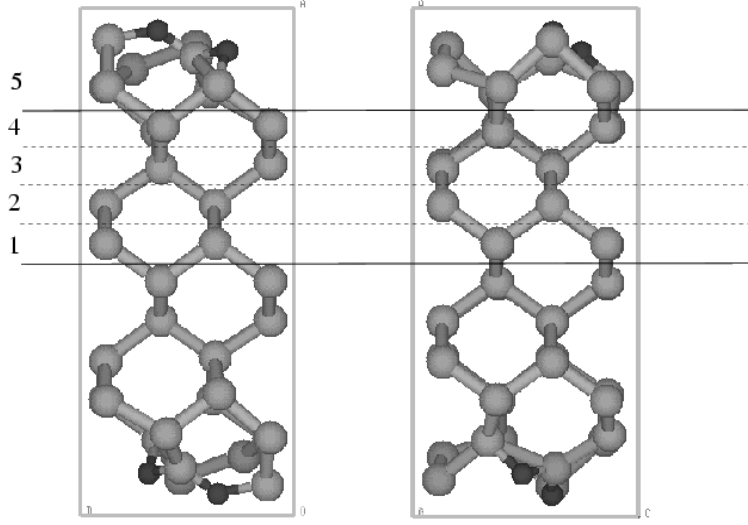


FIG. 5: Side view of the slab, and the slicing used for the layer-by-layer spectral decomposition performed according to the method of Ref. [22]. Left: view axis perpendicular to surface dimers. Right: view axis parallel to surface dimers. Darker spheres are used for oxygen, grey ones represent silicon atoms. The oxidized region is fully enclosed in slice 5.

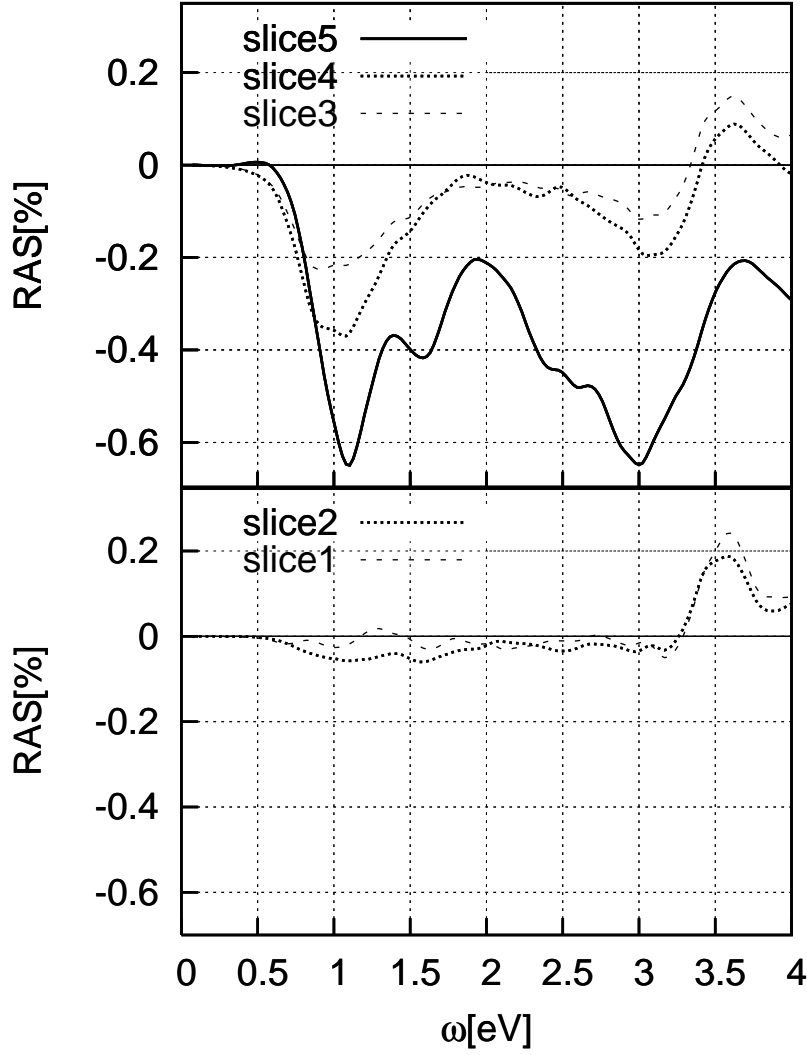


FIG. 6: Results of the layer-by-layer spectral decomposition, according to the slicing displayed in Fig. 5. The spectral feature at about 1.5 eV, recognized as an oxygen signature (see text), comes from the topmost slice only. In contrast, the main peaks at about 1 eV and 3 eV also include contributions from subsurface states (slice 3 and 4).

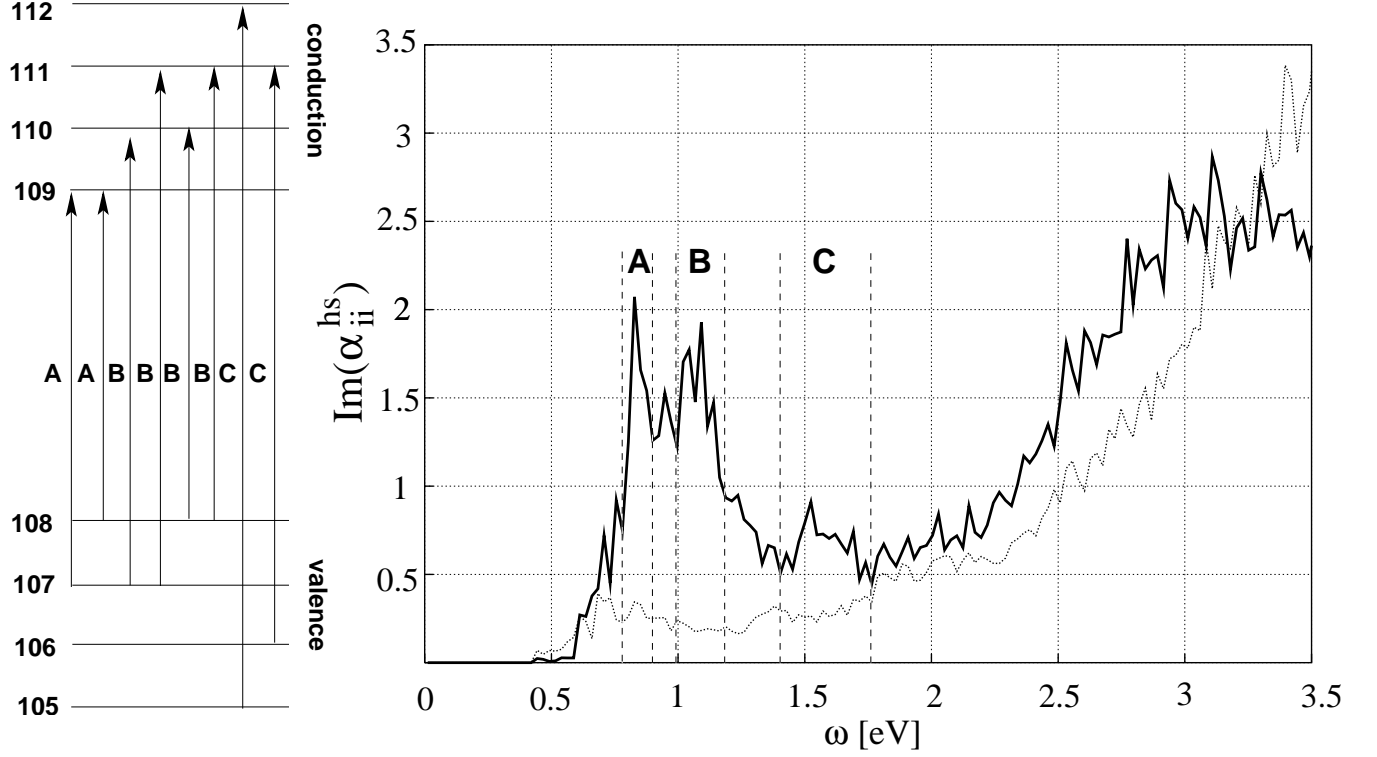


FIG. 7: Contributions of selected slab states involved in the strongest optical transitions for Si(100)-p(2x2):O, below 1.7 eV. Three energy windows, corresponding to the main spectral features in the imaginary part of the half-slab polarizability tensor $Im[\alpha_{ii}^{hs}]$, are studied: A ([0.8, 0.9] eV); B ([1.0, 1.15] eV); and C ([1.40, 1.75] eV). The full and dashed lines correspond to light polarization along the y and z directions, respectively. On the left, we represent schematically the slab states, below and above the Fermi level, and their originated transitions which carry the largest oscillator strength, and anisotropy, in regions A, B and C.

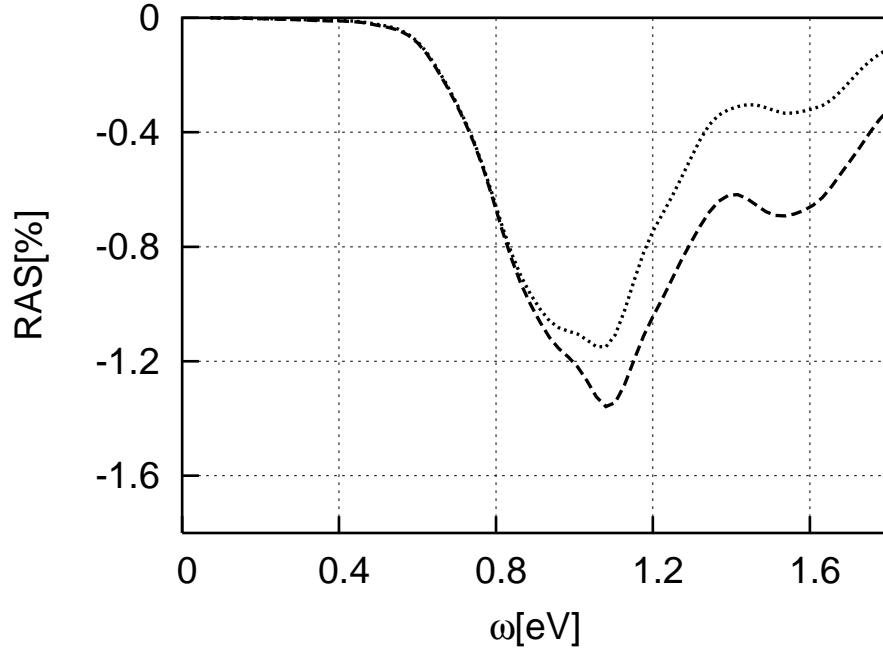


FIG. 8: Contribution of the eight surface states singled out in Fig. 7 to the Si(100)-p(2x2):O RAS. Dotted line: only 4+4 bands included in the summations of Eq. (4); dashed line: full calculation with 108+250 bands.